Available online at www.sciencedirect.com
ScienceDirect
Journal of Computational and Applied Mathematics 209 (2007) 1–21
JOURNAL OF COMPUTATIONAL AND APPLIED MATHEMATICS
www.elsevier.com/locate/cam

A simplified Fornberg-like method for the conformal mapping of multiply connected regions—Comparisons and crowding

N. Benchama[a], T.K. DeLillo[b,*], T. Hrycak[c], L. Wang[d]

[a]*Department of Mathematics, Minnesota State Community and Technical College, 1900 28th Ave. South, Moorhead, MN 56560, USA*
[b]*Department of Mathematics and Statistics, Wichita State University, Wichita, KS 67260-0033, USA*
[c]*Department of Mathematics, University of Vienna, Vienna, Austria*
[d]*Department of Mathematics and Computer Science, Fort Hays State University, 600 Park Street, Hays, KS 67601, USA*

Received 25 March 2004

Abstract

We present a new Fornberg-like method for the numerical conformal mapping of multiply connected regions exterior to circles to multiply connected regions exterior to smooth curves. The method is based on new, symmetric conditions for analytic extension of functions given on circular boundaries. We also briefly discuss a similar method due to Wegmann and compare some computations with both methods. Some examples of regions which exhibit crowding of the circles are also presented.

MSC: 30C30

Keywords: Numerical conformal mapping; Multiply connected regions; Crowding

1. Introduction

In this paper we present a new numerical method for conformally mapping unbounded multiply connected regions exterior to n nonoverlapping disks to unbounded regions exterior to n nonoverlapping Jordan curves ($n \geqslant 2$). The method was derived and studied in [1] and is essentially a "symmetrized" version of the method in [7]. The new setup makes the derivation, analysis, and coding much more straightforward than [7], especially for regions of connectivity greater than 2. The method is similar to [28] and we include some numerical comparisons. In addition, we discuss some examples where the geometry of the target region causes the circles in the computational region to nearly touch—an example of the so-called *crowding phenomenon* for multiply connected regions.

The new method uses the same Newton-like approach as the methods [7,28]. Each Newton iteration computes updates to the current approximations of the boundary correspondences and centers and radii of the circles. We show below that the inner linear system of equations at each Newton step is a discretization of the identity plus a compact operator and so the conjugate gradient method can be applied efficiently. For Fornberg-like methods, in general, using discretization by N-point trigonometric interpolation and FFTs leads to computational costs of $O(N \log N)$ for the simply and doubly

* Corresponding author. Department of Mathematical Sciences, Wichita State University, Wichita, Kansas 67260-0033, USA.
E-mail addresses: noureddine.benchama@minnesota.edu (N. Benchama), delillo@math.twsu.edu (T.K. DeLillo), tomasz.hrycak@univie.ac.at (T. Hrycak), l_wang@fhsu.edu (L. Wang).

0377-0427/$ - see front matter © 2006 Elsevier B.V. All rights reserved.
doi:10.1016/j.cam.2006.10.030

connected maps and $O(N^2)$ for the multiply connected maps. The fact that the inner linear systems for Fornberg-like methods are second kind (identity plus compact) integral operators was first recognized by Widlund [31] and Wegmann [25] for the simply connected case [9], and by [6,8] for the ellipse and doubly connected case. This attractive feature is hereby carried over to the multiply connected case. In this sense, the current work represents the culmination of research by the second author and his colleagues and students (see [5–8]) to extend Fornberg's original method [9] to increasingly complex geometries.

The interested reader is referred to [11,14,30] for introductions to the numerical methods for conformal mapping. Most methods for numerical conformal mapping compute the conformal moduli and the boundary correspondences between the canonical and target domains. Canonical domains whose boundaries are circles are popular alternatives, since the fast Fourier transform (FFT) can be applied. There are two approaches to deriving such methods. These two approaches have developed in parallel and use essentially the same linearization. One approach, due mainly to Wegmann, solves the inner linear systems for the Newton updates of the boundary correspondences and moduli as Riemann–Hilbert (RH) boundary value problems for the circular domains. The other approach, first proposed by Fornberg [9] for the simply connected case and extended by DeLillo et al., derives the inner linear systems from conditions on the Fourier (Laurent) coefficients which guarantee analytic extension of functions on the boundaries into the computational domain; see [2] for an overview. Both approaches have been developed for the following canonical domains: the unit disk [9,24,8], the annulus [8,18,26], the ellipse [5,6,27,15] and multiply connected circular domains [1,7,15,28,29].

Other methods for the multiply connected case have been developed. In [23], Wang has implemented the Koebe method [13,14] for the circle maps using both the exterior simply connected methods of Wegmann and of Fornberg [8] to successively map the exterior of each boundary component to the exterior of a disk. Prosnak has developed a linearly convergent projection method for this mapping problem; see [16,22,30]. The book [21] gives many applications of this method to problems in fluid dynamics. The reader can find more references for the multiply connected case in [7,28,30].

The remainder of this paper is organized as follows: we state the circle map problem in Section 2. In Section 3, we derive the analyticity conditions. After giving the linearization adopted in Section 4, we formulate the discrete problem as a linear system in Section 5. In Section 6, we provide an analysis of the inner linear system, showing that it is the discretization of a second kind operator. Wegmann's method for the circle map is outlined in Section 7 and some numerical examples comparing both methods are given in Section 8. In Section 9, we give a brief discussion of the crowding for the circle map and present some illustrative examples and estimates.

2. The circle map problem

We are seeking a conformal map f from the complement, D, of n closed nonintersecting disks, D_k, onto a region Ω which is exterior to n nonintersecting smooth Jordan curves, Γ_k, $1 \leqslant k \leqslant n$. Fig. 1 shows both the computational circle domain and the target domain. The following theorem, stated for the f^{-1} in [14], establishes the existence and uniqueness of the circle map under suitable normalization conditions.

Theorem 2.1. *Let Ω be a region of connectivity $n \geqslant 2$ in the extended complex plane such that $\infty \in \Omega$. Then there exists a unique circular region D of connectivity n and a unique one-to-one analytic function f in D satisfying*

$$f(z) = z + O(1/z) \quad \text{for } z \approx \infty, \tag{1}$$

such that $f(D) = \Omega$.

The boundaries of the circular disks D_k are the circles C_k with centers z_k and radii ρ_k and are parametrized by $c_k(\theta) := z_k + \rho_k e^{i\theta}$. The boundary of D is thus $C = C_1 + \cdots + C_n$. The boundary of Ω is $\Gamma = \Gamma_1 + \cdots + \Gamma_n$, where the boundaries Γ_k are parametrized by S, e.g., arclength, $\Gamma_k : \gamma_k = \gamma_k(S)$. For smooth γ_k, f extends smoothly to the boundary $f(C_k) = \Gamma_k$. The values of f on C will determine f everywhere. The *circle map problem* is, thus, to find the boundary correspondences $S = S_k(\theta)$ and the conformal moduli z_k, ρ_k such that

$$f(z_k + \rho_k e^{i\theta}) = \gamma_k(S_k(\theta)), \quad 1 \leqslant k \leqslant n, \tag{2}$$

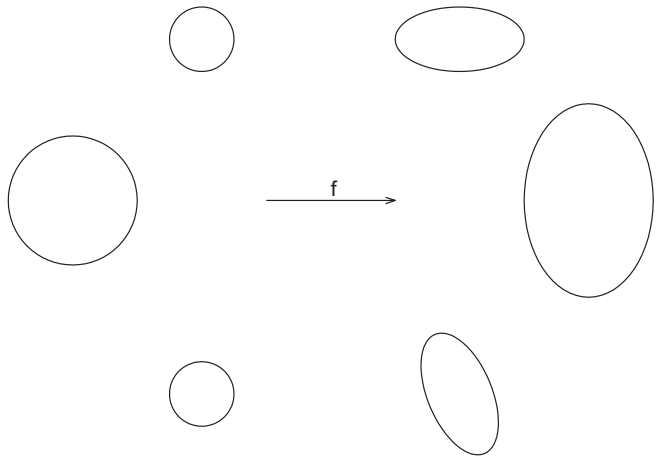

Fig. 1. Computational and target domains.

where f is analytic and has the normalization $f(z) = z + \mathrm{O}(1/z)$, $z \approx \infty$. The map f then has the form

$$f(z) = z + \sum_{k=1}^{n} \sum_{j=1}^{\infty} a_{k,-j} \left(\frac{\rho_k}{z - z_k} \right)^j, \tag{3}$$

where, for any integer j, $a_{k,j} := (1/2\pi) \int_0^{2\pi} f(z_k + \rho_k \mathrm{e}^{\mathrm{i}\theta}) \mathrm{e}^{-\mathrm{i}j\theta} \, \mathrm{d}\theta$ are the Fourier coefficients of the restriction of f to the boundary C_k.

3. Symmetrized analyticity conditions

We will follow closely the proof of Theorem 14.3b in [14] and Section 24 in [19] for establishing necessary and sufficient conditions for the analytic extension of a function in $\mathrm{Lip}(C)$ to the exterior of a simply connected domain.

Theorem 3.1. *A function $h \in \mathrm{Lip}(C)$, extends analytically to a function g in $D \cup \{\infty\}$ with $g(\infty) = 0$ if and only if for any $z \in \overline{D}^c$*

$$\frac{1}{2\pi\mathrm{i}} \int_C \frac{h(\zeta)}{\zeta - z} \, \mathrm{d}\zeta = 0. \tag{4}$$

Proof. We give a brief sketch of the proof. Define

$$g^+(\zeta) := \lim_{\substack{z \to \zeta \\ z \in D}} g(z) \quad \text{and} \quad g^-(\zeta) := \lim_{\substack{z \to \zeta \\ z \in \overline{D}^c}} g(z).$$

($\Rightarrow$): If g is analytic in $D \cup \{\infty\}$ ($g(\infty) = 0$) with $g^+(\zeta) = h(\zeta)$, then for $z \in \overline{D}^c$, the function $h(\zeta)/(\zeta - z)$ is analytic for $\zeta \in D$ and continuous for $\zeta \in C$. Therefore, we have

$$\frac{1}{2\pi\mathrm{i}} \int_C \frac{h(\zeta)}{\zeta - z} \, \mathrm{d}\zeta = \frac{1}{2\pi\mathrm{i}} \int_C \frac{g(\zeta)}{\zeta - z} \, \mathrm{d}\zeta = 0.$$

($\Leftarrow$): Let

$$g(z) := \frac{1}{2\pi\mathrm{i}} \int_C \frac{h(\zeta)}{\zeta - z} \, \mathrm{d}\zeta, \quad z \notin C$$

and assume $g(z) = 0$ for $z \in \overline{D}^c$. Then $g^-(\zeta) = 0$. By the Sokhotskyi formula [14, Theorem 14.1c] applied to the multiply connected domain D; see e.g. [19], we have

$$h(\zeta) = g^+(\zeta) - g^-(\zeta) = g^+(\zeta), \quad \zeta \in C.$$

Therefore, $h(\zeta)$ extends analytically to $g(z)$, $z \in D \cup \{\infty\}$. (Note that this definition of $g(z)$ gives $g(\infty) = 0$.) □

Now we are ready to state our main theorem which gives the necessary and sufficient conditions for analytic extension of the conformal map from the boundary into the domain in terms of the Fourier coefficients $a_{k,j}$. The conditions are a simpler, symmetrized version of the conditions used in [7]. We will need the binomial series

$$\frac{1}{(1-\Delta)^k} = \sum_{j=0}^{\infty} B_{k,j}\Delta^j, \quad |\Delta| < 1,$$

where the binomial coefficients $B_{k,j}$ are given by

$$B_{k,j} = \frac{k(k+1)\cdots(k+j-1)}{j!}, \quad k \geqslant 1, \quad j \geqslant 1, \quad B_{k,0} = 1.$$

Theorem 3.2. *Let D be the region exterior to the circles $C_k : z_k + \rho_k e^{i\theta}$, $1 \leqslant k \leqslant n$. Suppose $f \in \mathrm{Lip}(C)$ has the Fourier series representation*

$$f(z_k + \rho_k e^{i\theta}) = \sum_{j=-\infty}^{\infty} a_{k,j} e^{ij\theta}, \quad 1 \leqslant k \leqslant n.$$

Then f extends analytically into D with $f(z) = z + O(1/z)$ for $z \approx \infty$ if and only if

(i) *for all centers z_k*

$$\frac{1}{2\pi i}\int_C \frac{f(\zeta)-\zeta}{(\zeta - z_k)^j}\,d\zeta = 0, \quad j \geqslant 1; \tag{5}$$

(ii) *or equivalently,*

$$a_{k,j} - \left(\frac{\rho_k}{z_l - z_k}\right)^j \sum_{l\neq k}\sum_{v=0}^{\infty} B_{j+1,v}\left(\frac{\rho_l}{z_k - z_l}\right)^{v+1} a_{l,-v-1} = r_{k,j}, \quad j \geqslant 0, \tag{6}$$

where $r_{k,0} = z_k$, $r_{k,1} = \rho_k$ and $r_{k,j} = 0$ for $j \geqslant 2$.

Proof. To show the equivalence of condition (i), let $z \in \overline{D}^c$. Then $z \in D_k$ for some k and therefore $|(z-z_k)/(\zeta - z_k)| < 1$ for $\zeta \in C$. From Theorem 3.1, a necessary and sufficient condition for analytic extension of $h(\zeta) = f(\zeta) - \zeta$ is

$$\begin{aligned} 0 &= \frac{1}{2\pi i}\int_C \frac{h(\zeta)}{\zeta - z}\,d\zeta = \frac{1}{2\pi i}\int_C \frac{h(\zeta)}{(\zeta - z_k)(1 - ((z-z_k)/(\zeta - z_k)))}\,d\zeta \\ &= \sum_{j=0}^{\infty}(z - z_k)^j \frac{1}{2\pi i}\int_C \frac{h(\zeta)}{(\zeta - z_k)^{j+1}}\,d\zeta. \end{aligned}$$

Since z was arbitrary in $\overline{D}^c$, we must have

$$\frac{1}{2\pi i}\int_C \frac{f(\zeta)-\zeta}{(\zeta - z_k)^{j+1}}\,d\zeta = 0, \quad j \geqslant 0.$$

For the equivalence of condition (ii), we will apply condition (i) to $g(z) = f(z) - z = \mathrm{O}(1/z)$ for $z \approx \infty$. Then for $j \geqslant 0$

$$\begin{aligned}
0 &= \frac{1}{2\pi \mathrm{i}} \int_C \frac{g(\zeta)}{(\zeta - z_k)^{j+1}}\, \mathrm{d}\zeta \\
&= \frac{1}{2\pi \mathrm{i}} \int_C \frac{f(\zeta)}{(\zeta - z_k)^{j+1}}\, \mathrm{d}\zeta - \frac{1}{2\pi \mathrm{i}} \int_C \frac{\zeta}{(\zeta - z_k)^{j+1}}\, \mathrm{d}\zeta \\
&= \frac{1}{2\pi \mathrm{i}} \int_{C_k} \frac{f(\zeta)\, \mathrm{d}\zeta}{(\zeta - z_k)^{j+1}} - \frac{1}{2\pi \mathrm{i}} \int_{C_k} \frac{\zeta\, \mathrm{d}\zeta}{(\zeta - z_k)^{j+1}} + \sum_{l \neq k} \frac{1}{2\pi \mathrm{i}} \int_{C_l} \frac{f(\zeta)\, \mathrm{d}\zeta}{(\zeta - z_k)^{j+1}},
\end{aligned}$$

since

$$\frac{1}{2\pi \mathrm{i}} \int_{C_l} \frac{\zeta}{(\zeta - z_k)^{j+1}}\, \mathrm{d}\zeta = 0 \quad \text{for } l \neq k, \quad j \geqslant 0.$$

Next note that

$$\frac{1}{2\pi \mathrm{i}} \int_{C_k} \frac{\zeta}{(\zeta - z_k)}\, \mathrm{d}\zeta = z_k := y_{k,0}, \quad \frac{1}{2\pi \mathrm{i}} \int_{C_k} \frac{\zeta}{(\zeta - z_k)^2}\, \mathrm{d}\zeta = 1 := y_{k,1},$$

and

$$\frac{1}{2\pi \mathrm{i}} \int_{C_k} \frac{\zeta}{(\zeta - z_k)^{j+1}}\, \mathrm{d}\zeta = 0 := y_{k,j}, \quad j \geqslant 2.$$

The above conditions can therefore be written as

$$\frac{1}{2\pi \mathrm{i}} \int_{C_k} \frac{f(\zeta)}{(\zeta - z_k)^{j+1}}\, \mathrm{d}\zeta + \sum_{l \neq k} \frac{1}{2\pi \mathrm{i}} \int_{C_l} \frac{f(\zeta)}{(\zeta - z_k)^{j+1}}\, \mathrm{d}\zeta = y_{k,j}.$$

Substituting $\zeta = z_k + \rho_k \mathrm{e}^{\mathrm{i}\theta}$, $\mathrm{d}\zeta = \mathrm{i}\rho_k \mathrm{e}^{\mathrm{i}\theta}\, \mathrm{d}\theta$, with $0 \leqslant \theta \leqslant 2\pi$, we have

$$\int_{C_k} \frac{f(\zeta)\, \mathrm{d}\zeta}{(\zeta - z_k)^{j+1}} = \int_0^{2\pi} \frac{f(z_k + \rho_k \mathrm{e}^{\mathrm{i}\theta})}{(\rho_k \mathrm{e}^{\mathrm{i}\theta})^{j+1}} \mathrm{i}\rho_k \mathrm{e}^{\mathrm{i}\theta}\, \mathrm{d}\theta = \frac{2\pi \mathrm{i} a_{k,j}}{\rho_k^j}. \tag{7}$$

Also, for $l \neq k$ and $\zeta \in C_l$, we have $|(\zeta - z_l)/(z_k - z_l)| < 1$ and therefore,

$$\begin{aligned}
\int_{C_l} \frac{f(\zeta)}{(\zeta - z_k)^{j+1}}\, \mathrm{d}\zeta &= \mathrm{i}\rho_l \int_0^{2\pi} \frac{f(z_l + \rho_l \mathrm{e}^{\mathrm{i}\theta}) \mathrm{e}^{\mathrm{i}\theta}\, \mathrm{d}\theta}{(z_l + \rho_l \mathrm{e}^{\mathrm{i}\theta} - z_k)^{j+1}} \\
&= \mathrm{i}\rho_l \int_0^{2\pi} \frac{f(z_l + \rho_l \mathrm{e}^{\mathrm{i}\theta}) \mathrm{e}^{\mathrm{i}\theta}\, \mathrm{d}\theta}{(z_l - z_k)^{j+1} (1 - (\rho_l \mathrm{e}^{\mathrm{i}\theta}/(z_k - z_l)))^{j+1}} \\
&= \frac{\mathrm{i}\rho_l}{(z_l - z_k)^{j+1}} \sum_{v=0}^{\infty} B_{j+1,v} \left(\frac{\rho_l}{z_k - z_l} \right)^v \int_0^{2\pi} f(z_l + \rho_l \mathrm{e}^{\mathrm{i}\theta}) \mathrm{e}^{\mathrm{i}(v+1)\theta}\, \mathrm{d}\theta \\
&= -\frac{2\pi \mathrm{i}}{(z_l - z_k)^j} \sum_{v=0}^{\infty} B_{j+1,v} \left(\frac{\rho_l}{z_k - z_l} \right)^{v+1} a_{l,-v-1}.
\end{aligned} \tag{8}$$

Combining the above, we obtain condition (ii). □

In Section 5, we will discretize condition (ii) using N-point trigonometric interpolation and express the discrete form of the conditions in matrix form $P\underline{a} = \underline{r}$, where the $\underline{a}$ is an $nN \times 1$ vector with the discrete $a_{k,j}$'s as components. Combining these conditions with the linearizations in the next section will give us our inner linear system for the Newton updates of the boundary correspondences and centers and radii of the circles.

4. Linearization

Here we show how to linearize (2) with respect to f, $S_k(\theta)$, z_k, and ρ_k. We make an initial guess of $S_k(\theta)$ and correct it with the real, 2π-periodic function $U_k(\theta)$. We use the following linearization for $U_k(\theta)$:

$$\gamma_k(S_k(\theta) + U_k(\theta)) \approx \xi_k(\theta) + \gamma'(S_k(\theta))U_k(\theta), \quad 1 \leqslant k \leqslant n, \tag{9}$$

where $\xi_k(\theta) := \gamma_k(S_k(\theta))$. The linearization for the corrections δz_k and $\delta\rho_k$ to z_k and ρ_k is

$$(f + \delta f)(z_k + \delta z_k + (\rho_k + \delta\rho_k)\mathrm{e}^{\mathrm{i}\theta}) \approx f(z_k + \rho_k\mathrm{e}^{\mathrm{i}\theta}) + f'(z_k + \rho_k\mathrm{e}^{\mathrm{i}\theta})(\delta z_k + \delta\rho_k\mathrm{e}^{\mathrm{i}\theta}). \tag{10}$$

Equating the linear terms in (9) and (10) gives

$$(f + \delta f)(z_k + \rho_k\mathrm{e}^{\mathrm{i}\theta}) = \xi_k(\theta) + \gamma'(S_k(\theta))U_k(\theta) + \zeta_k(\theta)(\delta\rho_k + \delta z_k\mathrm{e}^{-\mathrm{i}\theta}), \tag{11}$$

where

$$\zeta_k(\theta) := -f'(z_k + \rho_k\mathrm{e}^{\mathrm{i}\theta})\mathrm{e}^{\mathrm{i}\theta} = \mathrm{i}\rho_k^{-1}\gamma'(S_k(\theta))S_k'(\theta). \tag{12}$$

These linearizations were first proposed in [18,7] and were rigorously justified in [28]. The conditions in Theorem 3.2 are applied to require that (11) are the boundary values of a function analytic in D. These conditions give linear equations for U_k, δz_k, $\delta\rho_k$. The discrete form of these equations is given next.

5. Discretization and matrix formulation

We will discretize our equations using N-point trigonometric interpolation. Let $\theta_j := (j-1)2\pi/N$, $j = 1, 2, \ldots, N$. For $1 \leqslant k \leqslant n$ and $1 \leqslant j \leqslant N$, we define the N-vectors and $N \times N$ matrices

$$F := [w^{-(j-1)(l-1)}]_{1 \leqslant l,j \leqslant N} = \text{FFT matrix} \quad \text{where } w = \mathrm{e}^{-\mathrm{i}2\pi/N},$$

$$E_k := \mathrm{diag}_j(\gamma'(S_k(\theta_j))),$$

$$\underline{\dot{S}}_k := \frac{N}{2\pi}[S_k(\theta_{j+1}) - S_k(\theta_j)],$$

$$\underline{U}_k := [U_k(\theta_j)],$$

$$\underline{\xi}_k := [\gamma_k(S_k(\theta_j))],$$

$$\underline{\zeta}_k := \mathrm{i}\rho_k^{-1}E_k\underline{\dot{S}}_k,$$

$$\underline{f}_k := [f(z_k + \rho_k\mathrm{e}^{\mathrm{i}\theta_j})],$$

$$\underline{a}_k := \frac{1}{N}F\underline{f}_k,$$

$$\underline{z} := [\mathrm{e}^{-\mathrm{i}\theta_j}].$$

Let $N = 2M$. We now use $a_{k,j}$ to denote the discrete Fourier coefficients. By the N-periodicity of the discrete Fourier coefficients $a_{k,j} = a_{k,j-N}$, we note that

$$\underline{a}_k = (a_{k,0}, a_{k,1}, \ldots, a_{k,N-1})^{\mathrm{T}} = (a_{k,0}, a_{k,1}, \ldots, a_{k,M-1}, a_{k,-M}, \ldots, a_{k,-2}, a_{k,-1})^{\mathrm{T}}.$$

We truncate the sums in the analyticity equations to M terms and we limit the number of equations to M by considering only $0 \leqslant j \leqslant M-1$. With the $a_{k,-j}$'s as given above, the system of discrete equations is

$$a_{k,j} - \sum_{l \neq k} \sum_{v=0}^{M-1} \left(\frac{\rho_k}{z_l - z_k} \right)^j B_{j+1,v} \left(\frac{\rho_l}{z_k - z_l} \right)^{v+1} a_{l,-v-1} = r_{k,j}, \tag{13}$$

where, $r_{k,0} = z_k$, $r_{k,1} = \rho_k$ and $r_{k,j} = 0$ for $2 \leqslant j \leqslant M-1$. Eq. (13) can be written in matrix form as follows:

$$P\underline{a} = P_1\underline{a_1} + P_2\underline{a_2} + \cdots + P_n\underline{a_n} = \underline{r}, \tag{14}$$

where we write $P = [P_1 \;\; P_2 \;\; \ldots \;\; P_n]$ and the $(nM \times 1)$ vector

$$\underline{r} := \begin{bmatrix} \underline{r}_1 \\ \underline{r}_2 \\ \vdots \\ \underline{r}_n \end{bmatrix},$$

with each $\underline{r}_k$ given by

$$\underline{r}_k := (z_k, \rho_k, 0, 0, \ldots, 0)^{\mathrm{T}} \in C^{M \times 1}.$$

Each P_k has the following block structure:

$$P_k = \begin{bmatrix} 0 & P_{1,k} \\ \vdots & \vdots \\ 0 & P_{k-1,k} \\ I & 0 \\ 0 & P_{k+1,k} \\ \vdots & \vdots \\ 0 & P_{n,k} \end{bmatrix},$$

where for $l \neq k$, the submatrices $P_{l,k}$ are all of order $M \times M$ with entries $(\rho_k/(z_l - z_k))^j B_{j+1,v} (\rho_l/(z_k - z_l))^{v+1}$ properly arranged. (Details about the submatrices $P_{l,k}$ can be found in [1].)

The linearization (11) can be written in matrix form

$$N\underline{a}_k = F\underline{f}_k = F\underline{\xi}_k + FE_k\underline{U}_k + \delta\rho_k F\underline{\zeta}_k + \delta z_k F(\underline{z} * \underline{\zeta}_k),$$

where $*$ denotes the Hadamard product.

For convenience, we present for the matrix formulation of our equations for connectivity $n = 2$. The generalization to arbitrary n is straightforward. Using block matrix notation, the analyticity conditions can be written:

$$[P_1 \;\; P_2] \begin{bmatrix} \underline{a}_1 \\ \underline{a}_2 \end{bmatrix} = \begin{bmatrix} \underline{r}_1 \\ \underline{r}_2 \end{bmatrix}. \tag{15}$$

Inserting the linearization conditions into (15) we obtain:

$$\begin{aligned} &P_1(FE_1\underline{U}_1 + \delta\rho_1 F\underline{\zeta}_1 + F(\underline{z} * \underline{\zeta}_1))(\mathrm{Re}\,\delta z_1 + \mathrm{iIm}\,\delta z_1) \\ &\quad + P_2(FE_2\underline{U}_2 + \delta\rho_2 F\underline{\zeta}_2 + F(\underline{z} * \underline{\zeta}_2))(\mathrm{Re}\,\delta z_2 + \mathrm{iIm}\,\delta z_2) = \underline{g}, \end{aligned} \tag{16}$$

where

$$\underline{g} := -[P_1 \;\; P_2] \begin{bmatrix} F\underline{\xi}_1 \\ F\underline{\xi}_2 \end{bmatrix} + \begin{bmatrix} \underline{r}_1 \\ \underline{r}_2 \end{bmatrix}. \tag{17}$$

If we define the M-vectors

$$\underline{w}_k = P_k F\underline{\zeta}_k, \quad \underline{wz}_k = P_k F(\underline{z} * \underline{\zeta}_k), \quad k = 1, 2,$$

the matrices

$$P = [P_1 \;\; P_2], \quad W = [\underline{w}_1 \;\; \underline{w}_2 \;\; \underline{wz}_1 \;\; \mathrm{i}\underline{wz}_1 \;\; \underline{wz}_2 \;\; \mathrm{i}\underline{wz}_2]$$

as well as the $(2N+6)\times 1$ vector of unknowns

$$\underline{U} = \begin{bmatrix} \underline{U}_1 \\ \underline{U}_2 \\ \delta\rho_1 \\ \delta\rho_2 \\ \mathrm{Re}\,\delta z_1 \\ \mathrm{Im}\,\delta z_1 \\ \mathrm{Re}\,\delta z_2 \\ \mathrm{Im}\,\delta z_2 \end{bmatrix}$$

then our system takes the form

$$D\underline{U} := [P \;\; W] \begin{bmatrix} F & 0 & 0 \\ 0 & F & 0 \\ 0 & 0 & I \end{bmatrix} \begin{bmatrix} E_1 & 0 & 0 \\ 0 & E_2 & 0 \\ 0 & 0 & I \end{bmatrix} \underline{U} = \underline{g}. \tag{18}$$

Taking the "normal" equations and using the fact that $\underline{U}$ is real gives us

$$\frac{2}{N}\,\mathrm{Re}(D^H D)\underline{U} = \frac{2}{N}\,\mathrm{Re}(D^H \underline{g}), \tag{19}$$

which we write as

$$A\underline{U} = \underline{b},$$

where $A := (2/N)\,\mathrm{Re}(D^H D)$ and $\underline{b} = (2/N)\,\mathrm{Re}(D^H \underline{g})$. Notice that A is symmetric and positive (semi)definite. We will use the conjugate gradient method to solve this system for updating the boundary correspondences and the conformal moduli. The Newton update for kth component, at the ith Newton step is

$$\begin{aligned} S_k^{(i+1)}(\theta) &= S_k^{(i)}(\theta) + U_k^{(i)}(\theta), \\ \rho_k^{(i+1)} &= \rho_k^{(i)} + \delta\rho_k^{(i)}, \\ z_k^{(i+1)} &= z_k^{(i)} + \delta z_k^{(i)}. \end{aligned} \tag{20}$$

We now summarize the main parts of the algorithm:

- Input the boundary of each component.
- If the boundary is not given by an analytic formula, fit each component with a periodic spline of period Tl_k parametrized by (chordal) arclength S, as in [7]. This step produces the coefficients of the spline.
- Initialize the boundary correspondence by

$$S_k^{(0)}(\theta_j) = (j-1)Tl_k/N.$$

- Initialize ρ_k and z_k. The user can do this either by guess or by using a subroutine that finds the optimal values for r_k and z_k such that the circle best fits the curve of component k.
- Set the maximum number of iterations (NWT) for the Newton process and for the conjugate gradient (CG) method.
- Start the Newton iteration. For $1 \leqslant i \leqslant$ NWT, where i denotes the iteration number:
  (1) use the boundary representation to interpolate the boundary at N points;
  (2) form $\underline{\dot{S}}_k$, E_k, $\underline{\xi}_k$, $\underline{\zeta}_k$, $\underline{f}_k$, $\underline{a}_k$, $\underline{b}$, W;
  (3) form the nonzeros blocks of the matrix P;
  (4) solve $A\underline{U} = \underline{b}$ by the conjugate gradient method (multiplication by A can be done efficiently by successively applying each factor);
  (5) update (20) at the mesh points $\theta = \theta_j$.

6. Analysis of the inner linear system

In this section, we will analyze the matrix A and show that the eigenvalues are well-grouped around 1, except for a few outliers. We will assume that S is arclength, so that $\gamma_k'(S) = \mathrm{e}^{\mathrm{i}\beta_k(S)}$, where β_k is the argument of the unit tangent. Again, we will only consider the case $n = 2$. Extension to general n is straightforward. We have

$$A = \frac{2}{N}\,\mathrm{Re}(D^H D) = \begin{bmatrix} A_{11} & A_{12} & X_1 \\ A_{21} & A_{22} & X_2 \\ X_1^{\mathrm{T}} & X_2^{\mathrm{T}} & W^H W \end{bmatrix}, \tag{21}$$

where $A_{ij} := (2/N)\,\mathrm{Re}(E_i^H F^H P_i^H P_j F E_j)$ and $X_i := (2/N)\,\mathrm{Re}(E_i^H F^H P_i^H W)$. To explain the overall distribution of the eigenvalues of A, it is sufficient to study those of the leading principal submatrix

$$\widehat{A} = \begin{bmatrix} A_{11} & A_{12} \\ A_{21} & A_{22} \end{bmatrix}.$$

By standard theorems in matrix theory, the eigenvalues of A and $\widehat{A}$ will interlace. Recall that

$$[P_1 \;\; P_2] = \begin{bmatrix} I & 0 & 0 & P_{1,2} \\ 0 & P_{2,1} & I & 0 \end{bmatrix}.$$

Therefore,

$$\begin{bmatrix} P_1^H \\ P_2^H \end{bmatrix} [P_1 \;\; P_2] = \begin{bmatrix} P_1^H P_1 & P_1^H P_2 \\ P_2^H P_1 & P_2^H P_2 \end{bmatrix} = \begin{bmatrix} I & 0 & 0 & P_{1,2} \\ 0 & P_{2,1}^H P_{2,1} & P_{2,1}^H & 0 \\ 0 & P_{2,1} & I & 0 \\ P_{1,2}^H & 0 & 0 & P_{1,2}^H P_{1,2} \end{bmatrix}.$$

We can decompose $P_1^H P_1$

$$P_1^H P_1 = \begin{bmatrix} I & 0 \\ 0 & P_{2,1}^H \end{bmatrix} \begin{bmatrix} I & 0 \\ 0 & P_{2,1} \end{bmatrix} = \begin{bmatrix} I & 0 \\ 0 & P_{2,1}^H P_{2,1} \end{bmatrix} = I_+ + \Delta_2, \tag{22}$$

where

$$\Delta_2 = \begin{bmatrix} 0 & 0 \\ 0 & P_{21}^H P_{21} \end{bmatrix} \quad \text{and} \quad I_+ = \begin{bmatrix} I & 0 \\ 0 & 0 \end{bmatrix}.$$

Next note that $A_{11} = (2/N)\,\mathrm{Re}(E_1^H F^H P_1^H P_1 F E_1)$ can be decomposed into two parts:

$$A_{11} = \frac{2}{N}\,\mathrm{Re}(E_1^H F^H I_+ F E_1) + \frac{2}{N}\,\mathrm{Re}(E_1^H F^H \Delta_2 F E_1) = A_{11}^{(1)} + A_{11}^{(2)}. \tag{23}$$

The matrix $A_{11}^{(2)} := (2/N)\,\mathrm{Re}(E_1^H F^H \Delta_2 F E_1)$ and the remaining matrices, A_{12} and A_{21}, are discretizations of compact operators, since they are the product of bounded operators and the integral operators with continuous kernels. The matrix $A_{11}^{(1)} := (2/N)\,\mathrm{Re}(E_1^H F^H I_+ F E_1)$ is the discretization of the $I + R$ where I is the identity and R is a compact operator as shown next. Following paper [8], one can see that $A_{11}^{(1)}$ is the discretization of

$$\mathrm{Re}(\mathrm{e}^{-\mathrm{i}\beta_1}(I + \mathrm{i}K + J)\mathrm{e}^{\mathrm{i}\beta_1}) = I + R,$$

where $R = \mathrm{Re}(\mathrm{e}^{-\mathrm{i}\beta_1}(\mathrm{i}K + J)\mathrm{e}^{\mathrm{i}\beta_1})$. Here K is the conjugation operator for the disk and $Jh = (1/2\pi)\int_0^{2\pi} h(\theta)\,\mathrm{d}\theta$. For each function h in $L_2(0, 2\pi)$, the operator R can be written as a Fredholm integral operator

$$Rh(\theta) = \frac{1}{2\pi}\int_0^{2\pi} h(\phi)\frac{\sin(((\theta - \phi)/2) - (\beta_1(\phi) - \beta_1(\theta)))}{\sin((\theta - \phi)/2)}\,\mathrm{d}\phi.$$

For γ sufficiently smooth, the operator R is a symmetric compact operator on L_2; see [25, Section 4]. A_{22} can clearly be analyzed in the same way. As a consequence, the eigenvalues cluster around 1. This feature carries over to the block matrix A.

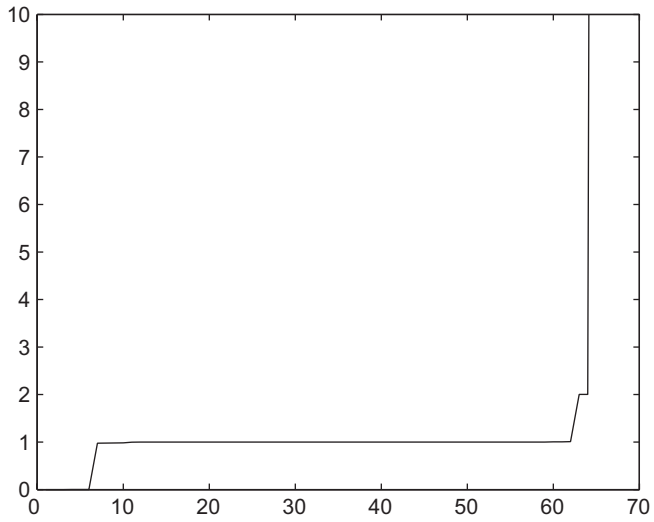

Fig. 2. Grouping of the eigenvalues around 1 for two circles.

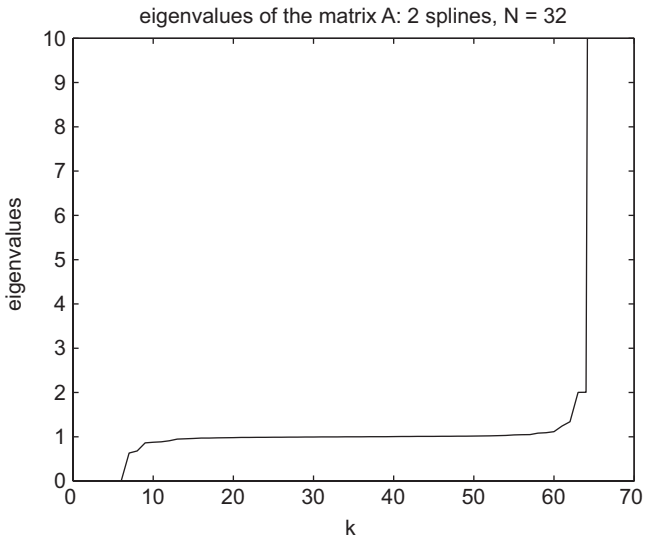

Fig. 3. Grouping of the eigenvalues around 1 for splines.

We present two plots showing the grouping of eigenvalues around 1 for two different geometries with $N = 32$. The first is Fig. 2 corresponding to a domain bounded by circles, so that f is the identity. We see a strong grouping around 1. Fig. 3 shows the grouping of the eigenvalues for a noncircular target domain bounded by cubic splines. The large outlying eigenvalues are associated with the W blocks.

7. Wegmann's method

In this section we briefly describe another method for conformal mapping of multiply connected regions using Wegmann's approach using RH problems (see [28,29]). In common with the Fornberg-like method, this method solves the circle map problem, i.e., finding the centers z_k and radii ρ_k $(1 \leqslant k \leqslant n)$ and boundary correspondences $S_k(\theta)$ such that

$$f(z_k + \rho_k e^{-i\theta}) := \gamma_k(S_k(\theta)), \quad 1 \leqslant k \leqslant n.$$

(Note that, following [28], the parametrization is reversed.) Using the linearization

$$f(z_k+\rho_k e^{-i\theta})+\delta f(z_k+\rho_k e^{-i\theta})+f'(z_k+\rho_k e^{-i\theta})(\delta z_k+\delta\rho_k e^{-i\theta})=\gamma_k(S_k(\theta))+\gamma_k'(S_k(\theta))U_k,$$

where $\gamma_k'(S_k(\theta))=r_k(S_k(\theta))e^{i\beta_k(S_k(\theta))}$.

At each Newton iteration, Wegmann's method [24] requires the solution of two RH problems (24) and (25). f, δf, f', Y and Ψ are connected by $f'=\exp(Y)$ and $\Psi=(f+\delta f)/\exp(Y)$.

The algorithm for Wegmann's method is as follows:

- Given initial guesses $S_k^{(0)}$, $z_k^{(0)}$, $\rho_k^{(0)}$ for the boundary correspondences, centers and radii.
- For each Newton iteration $i=0,1,2,\ldots$
  (1) Compute $v_k(\theta)=\beta_k(S_k(\theta))+\theta+\pi/2$.
  (2) Solve the RH problem

$$\mathrm{Re}(iY+\lambda_k)=-v_k. \tag{24}$$

  (3) Calculate $F_k=\exp(-w_k-i\beta_k-i\lambda_k)\gamma_k$.
  (4) Solve the RH problem

$$\mathrm{Re}(e^{i\theta}\Psi(z_k+\rho_k e^{-i\theta})+a_k e^{i\theta}+\alpha_k)=\mathrm{Im}\,F_k, \tag{25}$$

  for analytic $\Psi(z)=z+O(1/z)$ at ∞.
  (5) Compute the updates

$$U_k(\theta)=-\frac{e^{w_k}}{r_k}(g_k+\mathrm{Re}\,F_k),$$
$$\delta z_k=a_k-\mathrm{res}_\infty Y,$$
$$\delta\rho_k=\alpha_k$$

  where $\mathrm{res}_\infty Y$ is the residue of Y at ∞.
  (6) Smooth U_k: for the interpolating trigonometric polynomial

$$U_k=\sum_{j=-N/2+1}^{N/2-1}\hat{a}_j e^{ij\theta}+\hat{a}_{N/2}\cos(N\theta/2),$$

  set $\hat{a}_j=0$ for $|j|\geqslant N/4+1$.
  (7) Update the boundary correspondences, centers, and radii by

$$S_k^{i+1}=S_k^i+U_k,$$
$$z_k^{i+1}=z_k^i+\delta z_k,$$
$$\rho_k^{i+1}=\rho_k^i+\delta\rho_k.$$

The RH problems (24) and (25) can be solved by the method of successive conjugation (see [28–30]) using the FFT [25]. We start with the form of the map, which is called here Ψ

$$\Psi(z)=\sum_{k=1}^{n}h_k(z)=\sum_{k=1}^{n}\sum_{m=1}^{\infty}b_{k,m}(z-z_k)^{-m}, \tag{26}$$

where $h_k(z):=\sum_{m=1}^{\infty}b_{k,m}(z-z_k)^{-m}$ is analytic in the exterior of D_k.

We describe briefly the method of successive conjugation as applied to our problem. Let l be a nonnegative integer and ψ_k be real functions. The general form of the RH problem is to solve

$$\mathrm{Re}(e^{ilt}\Psi(z_k+\rho_k e^{-i\theta})+a_{k,l}e^{ilt}+\cdots+a_{k,1}e^{it}+a_{k,0})=\psi_k,\quad 1\leqslant k\leqslant n \tag{27}$$

for an analytic function Ψ in D with $\Psi(\infty) = 0$, real numbers $a_{k,0}$ and complex numbers $a_{k,1}, \ldots, a_{k,l}$. To solve the problem iteratively, given initial guesses $h_k^{(0)} = 0$, we can use a Gauss–Seidel-like method for Eq. (27)

$$\begin{aligned}
&\mathrm{Re}(\mathrm{e}^{\mathrm{i}lt} h_k^{(k+1)}(z_k + \rho_k \mathrm{e}^{-\mathrm{i}\theta}) + a_{k,l}\mathrm{e}^{\mathrm{i}lt} + \cdots + a_{k,1}\mathrm{e}^{\mathrm{i}t} + a_{k,0}) \\
&\quad = \psi_k - \mathrm{Re}\left(\sum_{v<k} \mathrm{e}^{\mathrm{i}lt} h_v^{(k+1)}(z_k + \rho_k \mathrm{e}^{-\mathrm{i}\theta})\right) - \mathrm{Re}\left(\sum_{v>k} \mathrm{e}^{\mathrm{i}lt} h_v^{(k)}(z_k + \rho_k \mathrm{e}^{-\mathrm{i}\theta})\right) \\
&\quad = \sum_{m=-\infty}^{\infty} A_{k,m}\, \mathrm{e}^{\mathrm{i}mt},
\end{aligned}$$

where $\sum_{m=-\infty}^{\infty} A_{k,m}\mathrm{e}^{\mathrm{i}mt}$ is the Fourier series expansion of the *RHS*. It follows that

$$a_{k,0} = A_{k,0}, \quad a_{k,j} = 2A_{k,j}, \quad j = 1, \ldots, l, \tag{28}$$

$$b_{k,m} = 2\rho_k^m A_{k,m+l} \quad \text{for } m = 1, 2, \ldots\ . \tag{29}$$

The evaluation of Ψ is of primary importance since, if it is not carefully arranged, it can lead to a very slow computation. Below, we show how to evaluate Ψ in (26). The matrices $P_{k,l}$ arise naturally in this evaluation.

Using (29), we have

$$h_v(z) = 2\sum_{m=1}^{\infty} \rho_v^m A_{v,m+l}(z - z_v)^{-m}.$$

For $v = k$,

$$h_k(z_k + \rho_k \mathrm{e}^{-\mathrm{i}\theta}) = \sum_{m=1}^{\infty} 2A_{k,m+l}\mathrm{e}^{\mathrm{i}mt}$$

which can be computed efficiently by the FFT.

For $v \neq k$,

$$\begin{aligned}
h_v(z_k + \rho_k \mathrm{e}^{-\mathrm{i}\theta}) &= 2\sum_{m=1}^{\infty} \rho_v^m A_{v,m+l}(z_k + \rho_k \mathrm{e}^{-\mathrm{i}\theta} - z_v)^{-m} \\
&= 2\sum_{m=1}^{\infty}\sum_{j=0}^{\infty} \left(\frac{\rho_v}{z_k - z_v}\right)^m \left(\frac{\rho_k}{z_v - z_k}\right)^j A_{v,m+l} B_{m,j} \mathrm{e}^{-\mathrm{i}j\theta} \\
&= \sum_{j=0}^{\infty} \left[\left(\frac{\rho_k}{z_v - z_k}\right)^j \sum_{m=0}^{\infty} B_{j+1,m}\left(\frac{\rho_v}{z_k - z_v}\right)^{m+1} (2A_{v,m+l+1})\right] \mathrm{e}^{-\mathrm{i}j\theta} \\
&:= \sum_{j=0}^{\infty} a_j^{k,v} \mathrm{e}^{-\mathrm{i}j\theta}.
\end{aligned} \tag{30}$$

Numerically, we truncate the above equation to M (here $M := (N/2) - l - 1$) terms to get

$$a_j^{k,v} = \left(\frac{\rho_k}{z_v - z_k}\right)^j \sum_{m=0}^{M-1} B_{j+1,m}\left(\frac{\rho_v}{z_k - z_v}\right)^{m+1} (2A_{v,m+l+1})$$

for $j = 0, 1, \ldots, M-1$, then

$$\begin{bmatrix} a_0^{k,v} \\ a_1^{k,v} \\ \vdots \\ a_{M-1}^{k,v} \end{bmatrix} = -P_{k,v} \begin{bmatrix} 2A_{v,M+l} \\ 2A_{v,M+l-1} \\ \vdots \\ 2A_{v,l+1} \end{bmatrix}.$$

We have already seen how to compute the matrices $P_{k,v}$. As to $h_v(z_k + \rho_k e^{-i\theta})$, it is clear from (30) that it can be evaluated by the FFT.

8. Numerical examples

We now compare both methods on some numerical examples.

Example 1. We use the exact map f from [7], Section 6, modified to satisfy our normalization. f maps the exterior of two circles with centers 0, $(x_1 + x_2)/2$ and radii 1, $(x_1 - x_2)/2$ onto an unbounded doubly connected region. The map is a composition of elementary maps,

$$f(z) = f_5(f_4(f_3(f_2(f_1(z))))).$$

The first map f_1 is the fractional linear map

$$f_1(z) = \frac{z - a}{az - 1},$$

where

$$a = \frac{x_1x_2 + 1 + \sqrt{(x_1^2 - 1)(x_2^2 - 1)}}{x_1 + x_2}, \quad R = \frac{x_1x_2 - 1 - \sqrt{(x_1^2 - 1)(x_2^2 - 1)}}{x_1 - x_2},$$

and $1 < x_2 < x_1$.

$$f_2(z) = \beta z, \quad f_3(z) = z + 1/z, \quad f_4(z) = \frac{\beta}{\beta^2 + 1} z,$$

where $\beta R \gg 1$ so that the region is not too extreme. The final map f_5 is the fractional linear map

$$f_5(z) = (C_1 z + C_2)/(z + C_3),$$

where

$$C_1 = \frac{a^4 - \beta^2}{a(a^2 - \beta^2)}, \quad C_2 = -\frac{3a^2\beta^2 + a^2 - \beta^4 - 3\beta^2}{a^2\beta^2 + a^2 - \beta^2 - \beta^4}, \quad C_3 = -\frac{a^2 + \beta^2}{a(\beta^2 + 1)}.$$

In this example we use $x_1 = 2$, $x_2 = 3$, $\beta = 30$. The tolerance for the residuals in the inner iteration is 1.0e − 15. The initial guess for the boundary correspondence is given by $S_k(\theta) = \theta$. We let DF, DZ, and DR denote the maximum numerical errors for the boundary components, centers, and radii, respectively. From Tables 1 and 2, Wegmann's and Fornberg's methods attain similar discretization errors. The map is shown in Fig. 4.

Table 1
Discretization errors for Fornberg's method, Example 1

N	DF	DZ	DR
32	1.5e − 05	6.3e − 11	6.3e − 11
64	1.9e − 08	6.8e − 16	2.2e − 16
128	1.7e − 13	4.4e − 16	2.2e − 16
256	5.0e − 15	4.4e − 16	2.2e − 16

Tables 3 and 4 give the numerical errors for a poorer initial guess, $z = [-0.1 + 0.1i; 2.6 + 0.2i]$, $r = [0.8; 0.4]$, for the centers and radii. Fornberg's method is more sensitive to the initial guess than Wegmann's method. Fig. 5 uses the same initial guess. Smoothing by zeroing half of the Fourier coefficients, as suggested in [28], is useful for both methods. Wegmann's method exhibits convergence–divergence behavior in Fig. 5. Fornberg's method may need more Newton iterations to achieve the same accuracy in this case.

Table 2
Discretization errors for Wegmann's method, Example 1

N	DF	DZ	DR
32	1.5e − 05	3.1e − 10	1.0e − 10
64	1.9e − 08	2.2e − 16	2.2e − 16
128	1.4e − 13	6.0e − 16	2.2e − 16
256	2.6e − 15	5.0e − 16	2.2e − 16

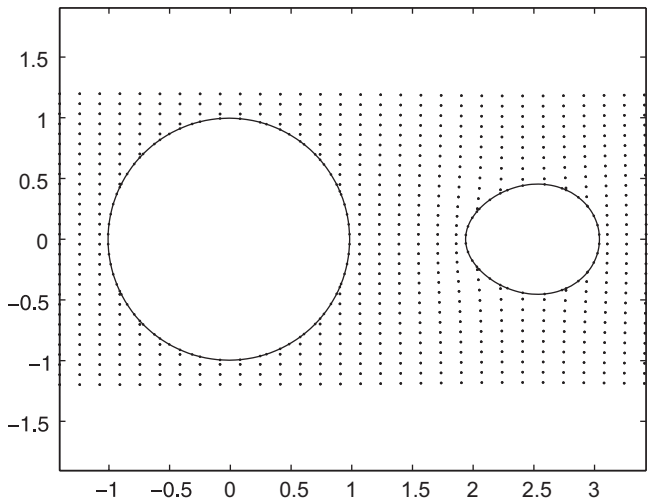

Fig. 4. Fornberg's method with $N = 128$, Example 1.

Table 3
Discretization errors for Fornberg's method, Example 1

N	DF	DZ	DR
32	1.5e − 05	1.4e − 10	6.4e − 11
64	2.4e − 08	1.5e − 11	1.4e − 13
128	2.4e − 09	1.7e − 12	8.0e − 15
256	5.6e − 10	2.0e − 13	3.3e − 16

Table 4
Discretization errors for Wegmann's method, Example 1

N	DF	DZ	DR
32	1.5e − 05	3.1e − 10	1.0e − 10
64	1.9e − 08	4.7e − 16	2.2e − 16
128	1.4e − 13	5.6e − 16	2.8e − 16
256	1.5e − 15	4.5e − 16	2.2e − 16

Example 2. A region of connectivity 5 bounded by arctanh, cassini oval, ellipse, inverted ellipse and sports ground curves. These boundaries are interpolated by periodic cubic splines parametrized by chordal arclength as described in [7]. In this example, we use $N = 128$. In Fig. 6, Fornberg's method shows a better error decay than Wegmann's method. The conformal map is displayed in Fig. 7.

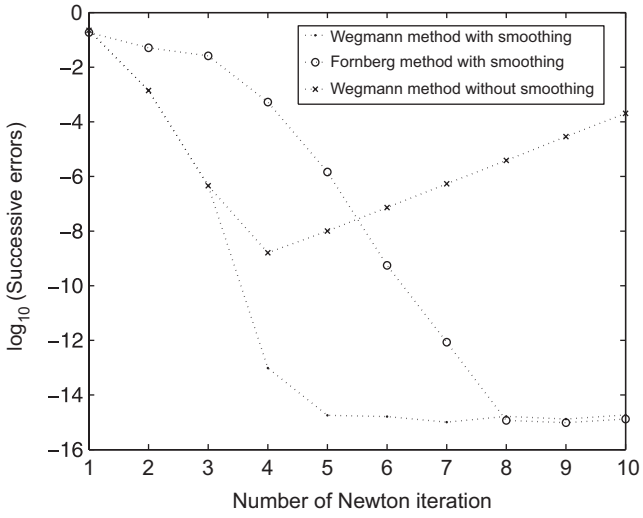

Fig. 5. Comparison of successive iteration errors, Example 1.

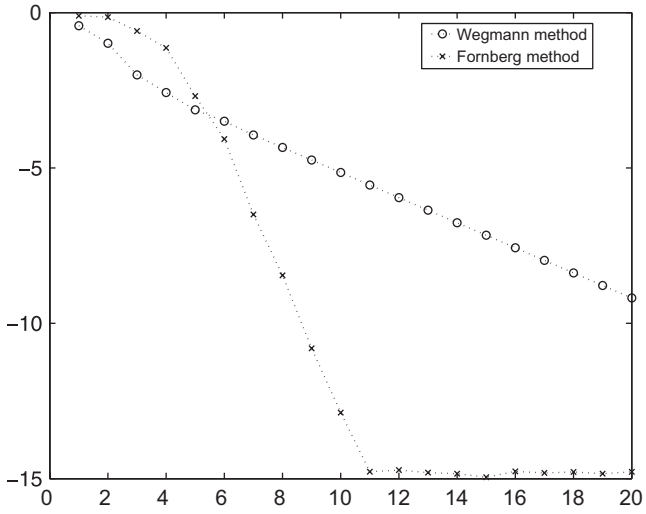

Fig. 6. Comparison of successive iteration errors, Example 2.

The inner iterations for Wegmann's method converges linearly. The inner iterations for Fornberg's method converges superlinearly. The outer Newton iterations converge nearly quadratically for both methods. Both algorithms require $O(N^2)$ work to do the matrix–vector multiplication.

9. Crowding for the circle map

The purpose of this section is to present some examples of the ill-conditioning, known as the crowding phenomenon, for conformal maps of multiply connected regions. A great deal of research has been done in the last 20 years on the crowding phenomenon, especially for the simply connected case; see [4] for references to some of the literature. Difficult cases for conformal mapping from exterior regions bounded by circles occur (i) when arcs of a circle map to the ends of elongated regions and (ii) when the circles are close to touching.

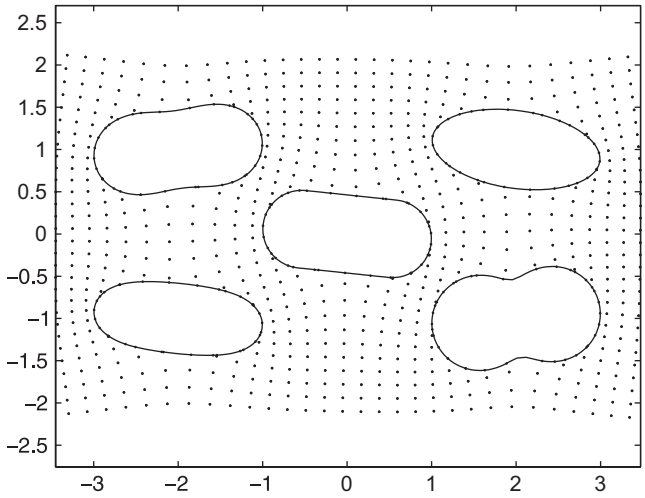

Fig. 7. Fornberg's method without smoothing, Example 2.

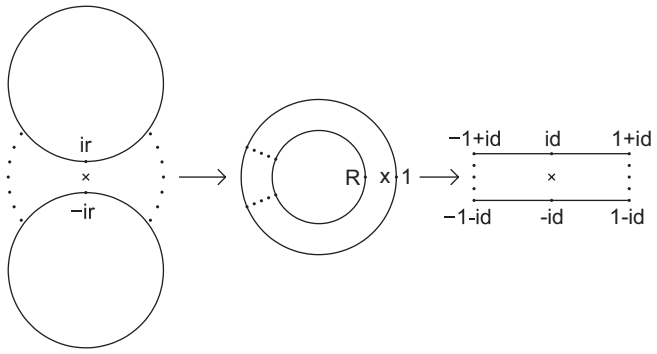

Fig. 8. Map of circles to annulus to parallel slits.

In this section, we are concerned with case (ii) when the circles are close to touching. This case also causes difficulty for the Koebe iteration [14,13,23] which uses simply connected maps to successively map the exterior of each boundary curve to the exterior of a circle. The numerical observations and linear convergence results, given in [14] for the Koebe map and in [29,7,1] for the inner linear systems in Newton-like methods, show that the convergence ratios for these methods are at most the inverse of the smallest magnification factor (greater than 1) which will cause two circles to touch. If any of the circles are already close to touching, this factor will be nearly 1 and the methods will converge very slowly. This situation also causes difficulties for computing solutions to related problems in potential flow and electrostatics, for instance, by the method of images [13], and requires special techniques [3].

We emphasize that the positions of the circles, though predetermined by the geometry, are not known in advance and must be computed. Multiply connected geometries which map to close-to-touching circles were noted by Halsey [13]. In particular, Halsey, [13], Fig. 5, gives an example of a map from the exterior of three thin ellipses with parallel major axes to the exterior of three nearly touching circles. In what follows we give two examples for which the maps and the associated measures of crowding are known explicitly, and compare our "exact"results with those computed by using our numerical method. Our two examples involve the mapping from two circles to two parallel and two collinear slits, respectively. In both of these cases, the crowding is due to elongated or narrow sections in the regions between the slits. In addition, we will compare the calculations for the slit regions to regions exterior to parallel and collinear ellipses with minor-to-major axis ratios of .1. Similar computational results using the Koebe iteration and initial attempts to derive crowding estimates are given in [23].

Table 5
Estimates r_{est} of r from (31) and computations r_{slit} using the new mapping method for two parallel slits; comparison with two parallel ellipses with $N = 128$

d	$r_{\text{est}} = \pi^2 d^2/2$	r_{slit}	$r_{\text{slit}}/r_{\text{est}}$	r_{ell}	$error_{\text{ell}}$
.15	.111	.072	.655	.071	9e − 4
.20	.197	.118	.601	.048	3e − 5
.30	.444	.228	.515	.136	8e − 5
.50	1.23	.499	.406	.367	2e − 4

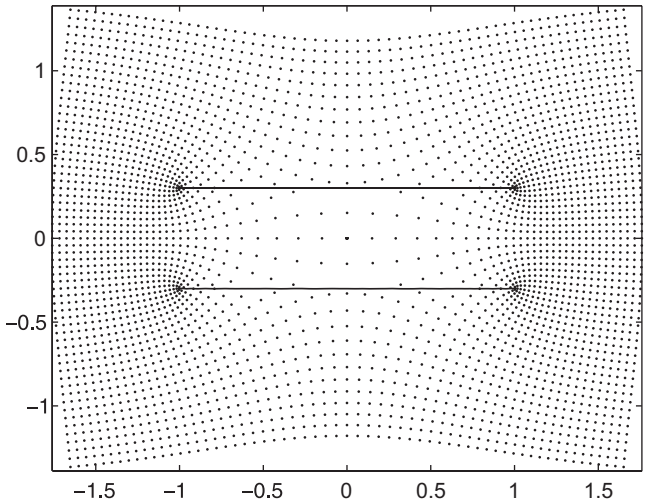

Fig. 9. Fornberg map to parallel slits with $d = 0.3$.

Example 1. Parallel slits and ellipses. For both of our examples, we will need the fractional linear transformation from the exterior of two circles to an annulus; see Fig. 8. Consider the region exterior to two circles with radii 1 and centers $\pm i(1 + r)$ in the plane. This region can be mapped explicitly, to an annulus of inverse modulus $R \approx 1 - \sqrt{8r}$ for small r; see e.g., [12, p. 1279]. For small r the image of the axe-shaped region bounded by the circles and the dotted lines in Fig. 8 will nearly cover the entire annulus. The annulus can be mapped periodically by log to a rectangle of aspect ratio $-\log R/2\pi \approx \sqrt{8r}/2\pi$ with the image of the origin mapped to the center of the rectangle.

The map from the region exterior to the parallel slits $[-1 + id, 1 + id]$, $[-1 - id, 1 - id]$ in Fig. 8 to an annulus is given in [17, Section 13.12] in terms of elliptic functions. For a small distance d the image of the rectangle between the slits will almost fill the entire annulus. Equating the inverse moduli of these two annuli, we find $1 - \sqrt{8r} \sim 1 - 2\pi d$. This gives the exact asymptotic crowding formula

$$r \sim \pi^2 d^2/2, \quad r, d \to 0. \tag{31}$$

The more elongated (or narrower) the channel between the slits, the closer the circles will be. (Note that the behavior is not exponential in the aspect ratio d of the channel as one might expect from elongated simply connected maps [4].)

A comparison of these estimates r_{est} with the value of r_{slit} computed using our new numerical conformal mapping method is given in Table 5. The circles are normalized to have radii equal to 1. Generally, the method requires smooth boundaries. However, the method gives good overall results for maps to exteriors of slits, even though a close inspection of the tips of the slits reveal inaccuracies. The map uses $N = 128$ Fourier points on each disk. Results for parallel ellipses r_{ell} with centers separated by $2d$ are also listed in Table 5. The errors $error_{\text{ell}}$ are the maximum pointwise errors in the boundary correspondences for the ellipses for $N = 128$ compared with the solution for $N = 256$. The errors in the centers and radii are usually 10^{-7}–10^{-9}. The change in the errors with d is not very severe or consistent, indicating that this form of crowding is not as great a problem as the case of elongated, simply connected regions. Figs. 9–11 display mappings of equally spaced Cartesian grid points in the circle domain in order to illustrate the distortions in the conformal maps.

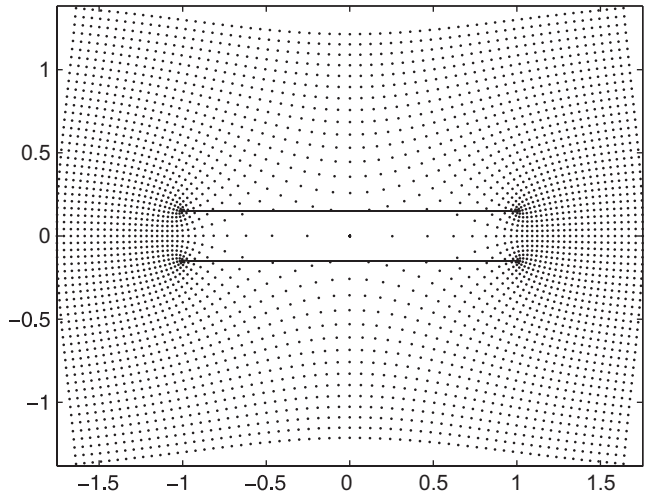

Fig. 10. Fornberg map to parallel slit with $d = 0.15$.

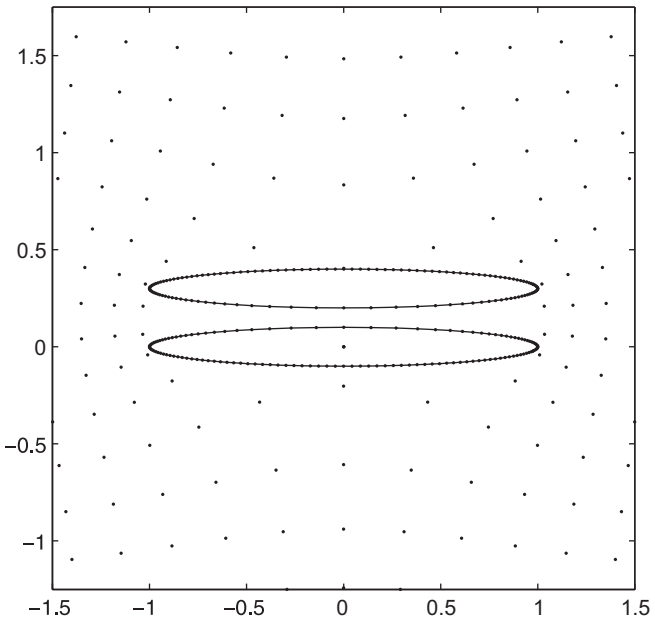

Fig. 11. Fornberg map to parallel ellipses with $d = 0.15$ showing distribution of mesh points ($N = 128$) on boundaries.

Example 2. Collinear slits and ellipses. Here we consider the region exterior of two collinear slits $[-2-d, -d]$, $[d, 2+d]$ in Fig. 12. The exact map from an annulus of outer radius 1 and inner radius $R < 1$ to the exterior of two slits $[1, 1/k]$ and $[-1/k, -1]$ is given in [17, Section 13.11], by $w = \mathrm{sn}((-2K/\log(R))\log(z/\sqrt{R}))$. Multiplication by $d = 2k/(1-k)$ maps to our region exterior to slits $[d, 2+d]$ and $[-2-d, -d]$. From the properties of sn, we have that $K \sim \pi/2$ and $K' \sim \log(4/k) \approx \log(8/d)$ as $d \to 0$; see, e.g. [4, Section 3(i), p. 801]. Using the map from the exterior disks to the annulus gives $2\pi/\sqrt{8r} \sim -2\pi/\log R \sim K'/K$ and finally

$$r \sim \frac{\pi^4}{8(\log(d/8))^2} \quad \text{or} \quad d \sim 8\mathrm{e}^{-\pi^2/\sqrt{8r}} \tag{32}$$

as $d \to 0$. Note that the crowding in this case is exponential in $-1/\sqrt{r}$.

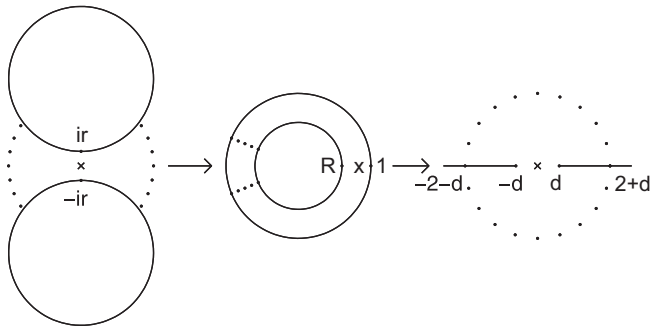

Fig. 12. Map of circles to annulus to collinear slits.

Table 6
Estimates r_{est} of r from 32 and computations r_{slit} using the new mapping method for two collinear slits; comparison with two collinear ellipses with $N = 128$

d	$r_{\text{est}} = \pi^4/8(\log(d/8))^2$	r_{slit}	$r_{\text{slit}}/r_{\text{est}}$	r_{ell}	$error_{\text{ell}}$
.025	.366	.407	1.11	.256	9e − 4
.05	.473	.517	1.09	.367	8e − 4
.1	.634	.693	1.09	.534	2e − 4
.2	.895	.982	1.09	.800	9e − 5

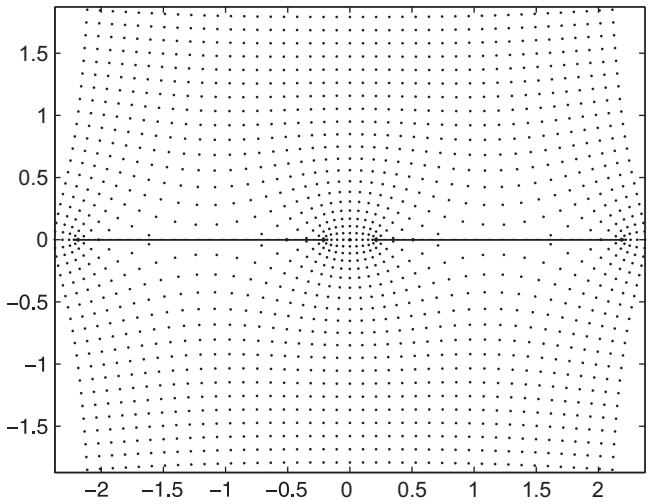

Fig. 13. Fornberg map to collinear slits with $d = 0.2$.

A comparison of this estimate with the value of r computed using our new Fornberg-like map is given in Table 6. The results are compared to collinear ellipses of minor-to-major axis ration .1 and length 2 with tips separated by $2d$. The errors are computed in the same way as the previous example with similar results. Mappings of equally spaced grid points are given in Figs. 13–15.

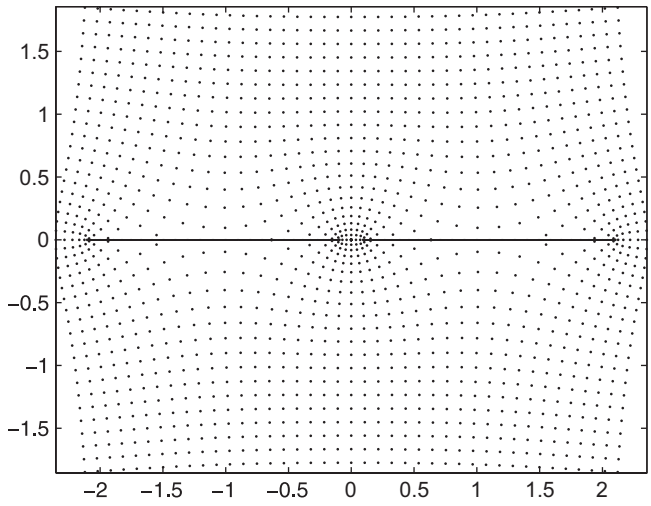

Fig. 14. Fornberg map to collinear slits with $d = 0.1$.

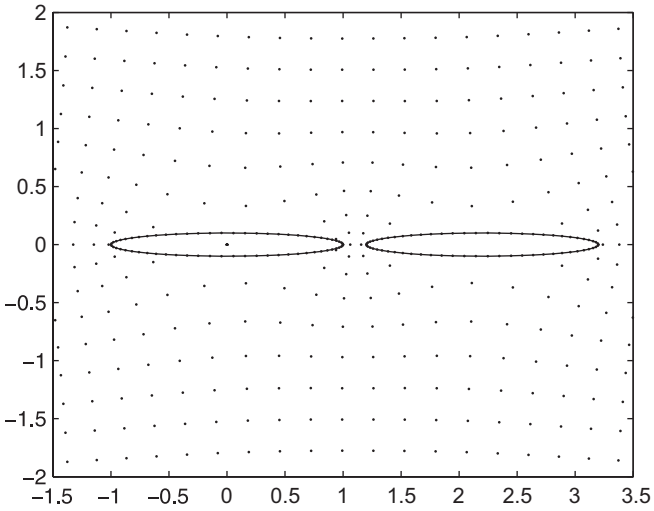

Fig. 15. Fornberg map to collinear ellipses with $d = 0.1$ showing distribution of mesh points ($N = 64$) on boundaries.

Acknowledgments

The authors are grateful to Rudolf Wegmann for pointing out the parallel slit example in [17]. This work was partially supported by an NSF EPSCoR Grant number 9874732 and ITR Grant number 0081270.

References

[1] N. Benchama, A simplified Fornberg-like method for the conformal mapping of multiply connected regions, Ph.D. Thesis, Mathematics Department, Wichita State University, 2003.

[2] N. Benchama, T.K. DeLillo, A brief overview of Fornberg-like methods for conformal mapping of simply and multiply connected regions, Bull. Malaysian Math. Sci. Soc., (second series) 26 (2003) 53–62.

[3] H. Cheng, L. Greengard, A method of images for the evaluation of electrostatic fields in systems of closely spaced conducting cylinders, SIAM J. Appl. Math. 88 (1998) 122–141.

[4] T.K. DeLillo, The accuracy of numerical conformal mapping methods: a survey of examples and results, SIAM J. Numer. Anal. 31 (1994) 788–812.
[5] T.K. DeLillo, A.R. Elcrat, A Fornberg-like conformal mapping method for slender regions, J. Comput. Appl. Math. 46 (1993) 49–64.
[6] T.K. DeLillo, A.R. Elcrat, J.A. Pfaltzgraff, Numerical conformal mapping methods based on Faber series, J. Comput. Appl. Math. 83 (1997) 205–236.
[7] T.K. DeLillo, M.A. Horn, J.A. Pfaltzgraff, Numerical conformal mapping of multiply connected regions by Fornberg-like methods, Numer. Math. 83 (1999) 205–230.
[8] T.K. DeLillo, J.A. Pfaltzgraff, Numerical conformal mapping methods for simply and doubly connected regions, SIAM J. Sci. Comput. 19 (1998) 155–171.
[9] B. Fornberg, A numerical method for conformal mappings, SIAM J. Sci. Statist. Comput. 1 (1980) 386–400.
[11] D. Gaier, Konstruktive Methoden der konformen Abbildung, Springer, Berlin, Göttingen, Heidelberg, 1964.
[12] M.D. Greenberg, Advanced Engineering Mathematics, Prentice-Hall, Englewood Cliffs, NJ, 1998.
[13] N.D. Halsey, Potential flow analysis of multielement airfoils using conformal mapping, Amer. Inst. Aeronautics Astronautics J. 17 (1979) 1281–1288.
[14] P. Henrici, Applied and Computational Complex Analysis, vol. III, Wiley, New York, 1986.
[15] M.A. Horn, Iterative methods applied to some problems in conformal mapping and potential theory, Ph.D. Thesis, Mathematics Department, Wichita State University, 1997.
[16] M.E. Klonowska, W.J. Prosnak, On an effective method for conformal mapping of multiply connected domains, Acta Mech. 119 (1996) 35–52.
[17] H. Kober, Dictionary of Conformal Representations, Dover Publications, New York, 1957.
[18] P. Luchini, F. Manzo, Flow around simply and multiply connected bodies: a new iterative scheme for conformal mapping, Amer. Inst. Aeronautics Astronautics J. 27 (1989) 345–351.
[19] N.I. Muskhelishvili, Singular Integral Equations, second ed., Dover, New York, 1992.
[21] W.J. Prosnak, Conformal representation of arbitrary multiconnected airfoils, Bull. Acad. Polish Sci. 25 (1977) 25–36.
[22] W.J. Prosnak, Computation of Fluid Motions in Multiply Connected Domains, G. Braun, Karlsruhe, 1987.
[23] L. Wang, Computational methods for two problems in potential theory, Ph.D. Thesis, Mathematics Department, Wichita State University, 2000.
[24] R. Wegmann, Convergence proofs and error estimates for an iterative method for conformal mapping, Numer. Math. 44 (1984) 435–461.
[25] R. Wegmann, On Fornberg's numerical method for conformal mapping, SIAM J. Numer. Anal. 23 (1986) 1199–1213.
[26] R. Wegmann, An iterative method for the conformal mapping of doubly connected regions, J. Comput. Appl. Math. 14 (1986) 79–98.
[27] R. Wegmann, Fast conformal mapping of an ellipse to a simply connected region, J. Comput. Appl. Math. 72 (1996) 101–126.
[28] R. Wegmann, Fast conformal mapping of multiply connected regions, J. Comput. Appl. Math. 130 (2001) 119–138.
[29] R. Wegmann, Constructive solution of a certain class of Riemann–Hilbert problems on multiply connected circular domains, J. Comput. Appl. Math. 130 (2001) 139–161.
[30] R. Wegmann, Methods for numerical conformal mapping, in: R. Kuehnau (Ed.), Handbook of Complex Analysis, Geometric Function Theory, vol. 2, Elsevier, Amsterdam, 2005, pp. 351–477.
[31] O. Widlund, On a numerical method for conformal mapping due to Fornberg, (c.1981) unpublished.

Further reading

[10] B. Fornberg, A numerical method for conformal mapping of doubly connected regions, SIAM J. Sci. Statist. Comput. 4 (1984) 771–783.
[20] Z. Nehari, Conformal Mapping, McGraw-Hill, New York, 1952.